Pyrene-Based Covalent Organic Frameworks for Photocatalytic Hydrogen Peroxide Production

Jiamin Sun,[a] Himanshu Sekhar Jena,[a] Chidharth Krishnaraj,[a] Kuber Singh Rawat,[b] Sara Abednatanzi,[a] Jeet Chakraborty,[a] Andreas Laemont,[a] Wanlu Liu,[a] Hui Chen,[a] Ying-Ya Liu,[c] Karen Leus,[a] Henk Vrielinck,[d] Veronique Van Speybroeck,[b] Pascal Van Der Voort*[a]

[a] Prof. P. Van Der Voort, J.M. Sun, Dr. H. Sekhar Jena, Dr. C. Krishnaraj, Dr. S. Abednatanzi, Dr. J. Chakraborty, A. Laemont, Dr. H. Chen, Dr. K. Leus
COMOC—Center for Ordered Materials, Organometallics and Catalysis
Department of Chemistry, Ghent University
Krijgslaan 281, building S3, 9000 Ghent, Belgium
E-mail: Pascal.Vandervoort@ugent.be

[b] Prof. V. Van Speybroeck, Dr. K. Singh Rawat
Center for Molecular Modeling (CMM), Ghent University
Technologiepark 46, 9052 Zwijnaarde, Belgium

[c] Prof. Ying-Ya, Liu
State Key Laboratory of Fine Chemicals
Dalian University of Technology
116023, Dalian, PR China

[d] Prof. H. Vrielinck
Department of Solid-State Sciences, Ghent University
Krijgslaan 281, building S1, 9000 Ghent, Belgium

Supporting information for this article is given via a link at the end of the document.

Abstract: Four highly porous covalent organic frameworks (COFs) containing pyrene units were prepared and explored for photocatalytic H_2O_2 production. The experimental studies are complemented by density functional theory calculations, proving that the pyrene unit is more active for H_2O_2 production than the bipyridine and (diarylamino)benzene units reported previously. H_2O_2 decomposition experiments verified that the distribution of pyrene units over a large surface area of COFs plays an important role in catalytic performance. The Py-Py-COF, though contains more pyrene units than other COFs, induces a high H_2O_2 decomposition due to a dense concentration of pyrene in small proximity over a limited surface area. Therefore, a two-phase reaction system (water-benzyl alcohol) was employed to inhibit H_2O_2 decomposition. This is the first report on applying pyrene-based COFs in a two-phase system for photocatalytic H_2O_2 generation.

Introduction

Hydrogen peroxide (H_2O_2), a versatile green chemical, is widely used in various fields such as disinfection, bleaching, chemical synthesis, and aerospace.[1] The global consumption of H_2O_2 is expected to reach up to 5.7 million tons by 2027.[2] Currently, an anthraquinone-based technique is applied for industrial H_2O_2 production by using Pd/Al_2O_3 as the catalyst.[2b] However, this approach is a multiple-step process that suffers from intensive energy consumption and substantial waste emission. The photocatalytic H_2O_2 production via a $2e^-$ oxygen reduction reaction (ORR) offers a sustainable way to mitigate these issues. In recent years, organic semiconductors particularly metal-free polymers, such as graphitic carbon nitride (g-C_3N_4),[3] linear conjugated polymers,[4] covalent triazine frameworks (CTFs),[5] and covalent organic frameworks (COFs)[6] have emerged as promising materials for photocatalytic H_2O_2 production. Among these catalysts, COFs as photocatalysts have received recent attention due to their large surface areas, superior tunability, visible-light harvesting properties, and good chemical stability.[7] Recently, we reported N,N,N′,N′-tetrakis(4-aminophenyl)-1,4-phenylenediamine (TAPD) based COFs as a first proof-of-principle to reduce oxygen to generate H_2O_2 under visible light irradiation via a $2e^-$ ORR pathway.[6d] Up to now, only a few COFs have been explored in photocatalytic H_2O_2 production, such as triphenylbenzene-based COFs,[6b] triazine-based COFs,[6a] bipyridine-based COFs,[6c] and very recently vinylene-linked triazine COFs.[8] Compared to the most widely studied g-C_3N_4, COFs exhibited a higher photoactivity for H_2O_2 production because of their highly porous conjugated scaffold in combination with their structural designability.

Pyrene is a well-known chromophore and an excellent electron donor. Its large π-conjugated structure ensures strong light-harvesting and rapid electron-transfer abilities.[9] Pyrene-based small organic molecules have been used for H_2O_2 production via a $2e^-$ ORR pathway.[10] Compared to organic molecules, pyrene-based COFs possess a large accessible surface area, an ordered porous crystalline structure, and numerous active surface sites over larger surface areas. The π-π stacking of the pyrene layers in the Z-direction further improves the conjugation of COFs and lowers the bandgap. Till now, pyrene-based COFs have shown considerable potential in photocatalytic hydrogen evolution and organic transformation reactions.[11]

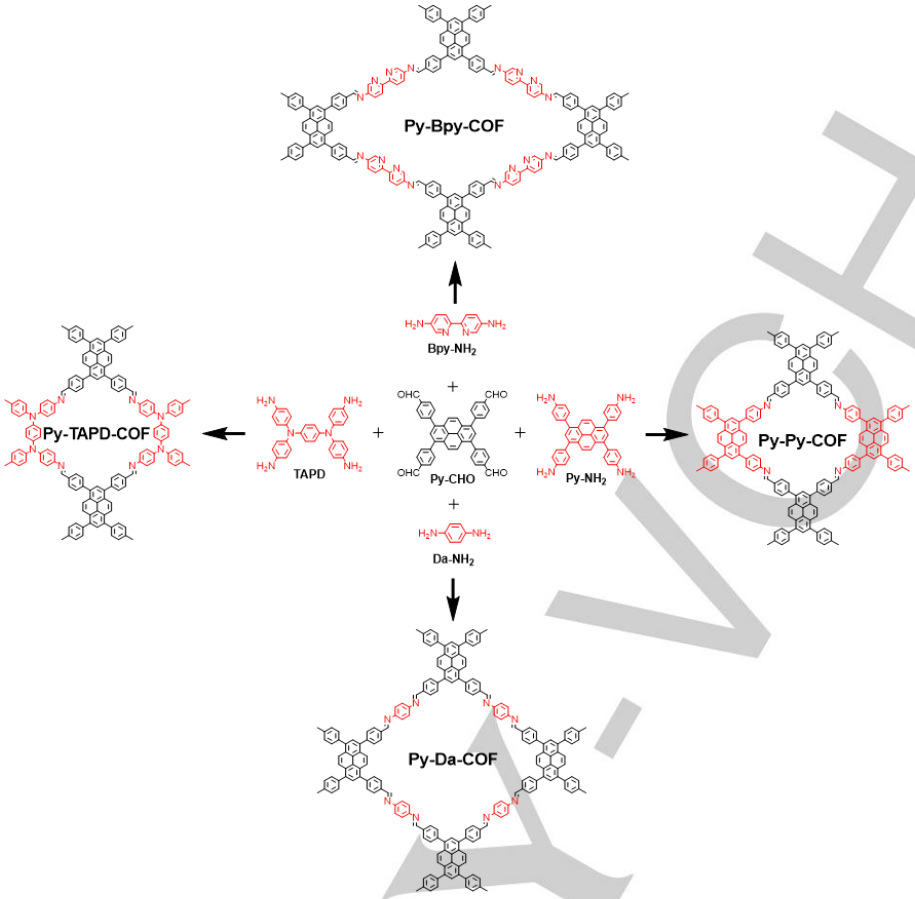

Scheme 1. Schematic illustration of the pyrene-based COFs.

Inspired by the beneficial features of COFs and the pyrene moiety, we synthesized four imine-linked COFs bearing the pyrene building unit 1,3,6,8-tetra(4-formylphenyl)pyrene (Py-CHO). Since TAPD and bipyridine (Bpy) units have shown to be good motifs for H_2O_2 generation,[6c] their overall synergistic effects in combination with pyrene units within COFs are investigated. For a comparison, Py-Py-COF (Py-CHO with 4,4',4'',4'''-(pyrene-1,3,6,8-tetrayl)tetraaniline (Py-NH_2)) and Py-Da-COF (Py-CHO with 1,4-diaminobenzene (Da-NH_2)) were prepared via Schiff-base condensation reactions. The photocatalytic performance of all four pyrene-based COFs for H_2O_2 production without/with a sacrificial agent was explored. We found that the distribution of pyrene units over large surface areas of COFs plays a significant role in their photocatalytic performance. COFs with electron-rich pyrene units are beneficial for H_2O_2 formation, however a high amount of pyrene units in close proximity induces severe H_2O_2 decomposition.

Results and Discussion

Four pyrene-based imine COFs were synthesized via a Schiff-base condensation reaction of Py-CHO with Da-NH_2, 2,2'-bipyridine-5,5'-diamine (Bpy-NH_2), TAPD or Py-NH_2 to obtain the corresponding Py-Da-COF, Py-Bpy-COF, Py-TAPD-COF, and Py-Py-COF, respectively (Scheme 1).[12] TAPD and Bpy are considered as the electron-rich reduction centers for O_2 binding which is a crucial step for H_2O_2 formation.[6c, 6d] To investigate the preferable O_2 binding sites on all four COFs, we analyzed the free adsorption energy of O_2 using density functional theory (DFT) calculations. Three possible adsorption sites are considered for each COF, also including the Bpy site in Py-Bpy-COF and the

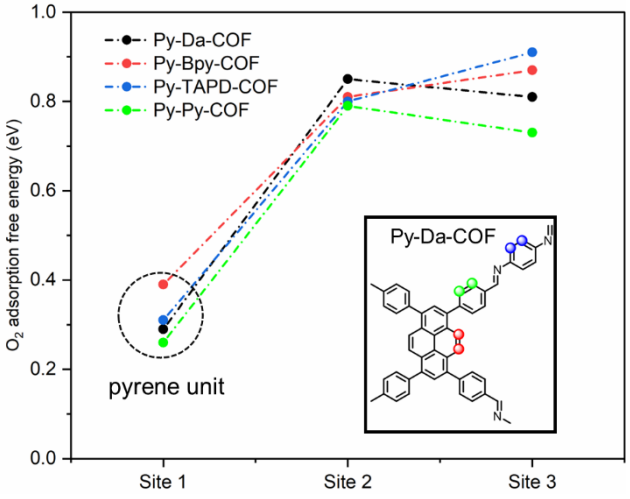

Figure 1. The calculated adsorption free energy of O_2 on different sites of all the pyrene-based COFs at the PBE-D3(BJ) level of theory. The inset shows all the three sites for Py-Da-COF, where site 1 is the pyrene unit, site 2 is the benzene moiety attached to the pyrene unit, and site 3 is remaining unit (Py, Da, TAPD or Bpy).

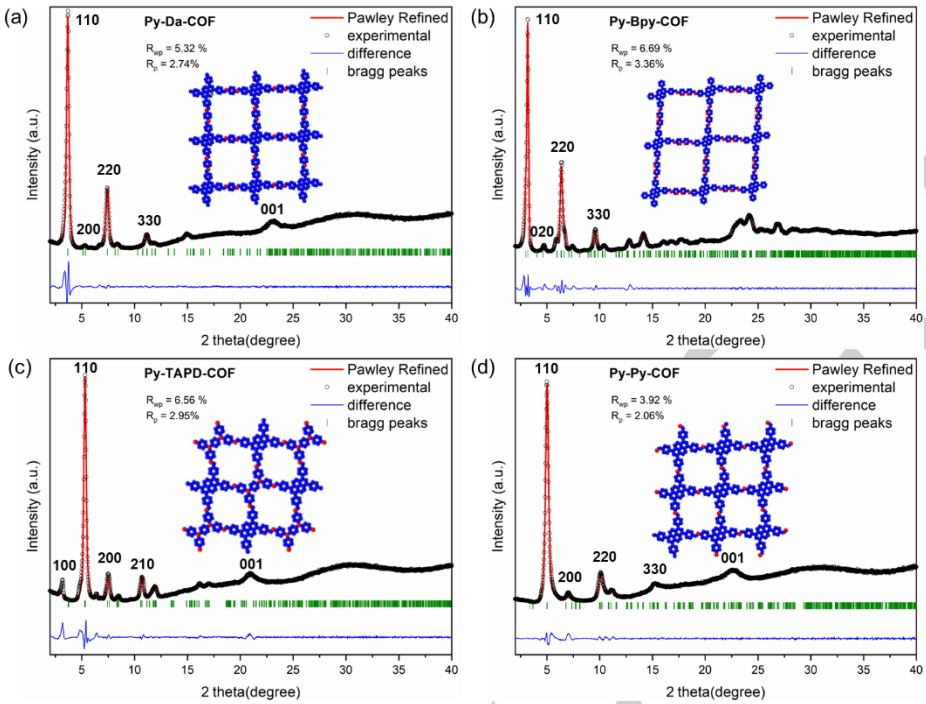

Figure 2. The PXRD patterns and Pawley refinements of (a) Py-Da-COF, (b) Py-Bpy-COF, (c) Py-TAPD-COF, and (d) Py-Py-COF. Inset images are modeled crystal structures. C, blue; H, white; N, red.

TAPD site in Py-TAPD-COF (site 1, pyrene unit; site 2, the benzene moiety attached to the pyrene unit; site 3, the remaining unit (Da, Bpy, TAPD or Py)). We found that in all COFs, O_2 adsorption is favored at the pyrene unit (site 1), corresponding to the small positive free energy of O_2 adsorption (Figure 1, S2-S5, and Table S1). And comparing within the COFs, O_2 binds stronger with Py-Py-COF (0.26 eV) compared to Py-Da-COF (0.29 eV), Py-Bpy-COF (0.39 eV), and Py-TAPD-COF (0.31 eV). These results suggest that the pyrene unit is the most active reduction center followed by Bpy and TAPD sites. Furthermore, we carried out Bader charge analysis to understand the charge transfer during the O_2 adsorption process. In the case of Py-Da-COF, the calculated Bader charges are -0.28 e, -0.31 e, and 0.64 e for site 1, site 2, and site 3, which decreased to 0.54 e, 0.66 e, and 1.68 e respectively after the O_2 adsorption, with a charge on the adsorbed O_2 of ~ -1 e (Table S2-S3). This suggests that charge transfer occurs from COFs to the O_2 molecule, and that the active site with the highest charge favors the O_2 adsorption. Site 1 (-0.28 e) has the highest charge among all the three sites in Py-Da-COF. This result agrees well with our calculated free energy of adsorption of O_2, showing that the site 1 is most favorable for O_2 adsorption. Similar trends were also found for the other studied COFs.

The crystallinity of the synthesized COFs was confirmed by powder X-ray diffraction (PXRD) and their structures were analyzed by experimental PXRD measurements combined with theoretical simulations. As shown in Figure 2a and 2b, Py-Da-COF and Py-Bpy-COF exhibit a sharp and intense diffraction peak below 5.0° (2θ), which corresponds to the (110) diffraction peak. Similarly, a sharp peak is observed at 5.3° or 5.0° in the PXRD patterns of Py-TAPD-COF and Py-Py-COF, respectively. According to the simulated patterns, the experimental PXRD patterns for all four COFs are consistent with the simulated eclipsed (AA) arrangement rather than staggered (AB) stacking (Figure S6). The models were geometrically optimized and the Pawley refinement against experimental PXRD data provides a good agreement (Py-Da-COF, R_p = 2.74%; Py-Bpy-COF, R_p = 3.36%; Py-TAPD-COF, R_p = 2.95%; Py-Py-COF, R_p = 2.06%). The high crystallinity combined with the AA stacking arrangement is beneficial for the transport of charge carriers.[6b, 13].

The imine bond formation of the COFs was verified by Fourier transform infrared spectroscopy (FT-IR). The characteristic C=N vibration bands are clearly observed at 1623, 1626, 1624, and 1627 cm^{-1} in the spectra of Py-Da-COF, Py-Bpy-COF, Py-TAPD-COF, and Py-Py-COF, respectively (Figure S7). To assess the porosity of all four COFs, argon (Ar) sorption measurements were performed at 87 K. As shown in Figure 3a and 3b, both Py-Da-COF and Py-Bpy-COF present a typical type IV isotherm. An obvious step is clearly observed at approximately P/P_0 = 0.1 and 0.18 in the isotherms of Py-Da-COF and Py-Bpy-COF respectively, indicating the presence of mesopores. The results of the pore size distribution (PSD) analysis of Py-Da-COF and Py-Bpy-COF using an Ar sorption-based quenched solid density functional theory (QSDFT) method show a narrow pore size distribution with a diameter of 2.6 and 3.0 nm respectively, which match well with the simulated values (2.5 and 2.8 nm). The Brunauer-Emmett-Teller (BET) surface area and total pore volume (at P/P_0 = 0.99) of Py-Da-COF and Py-Bpy-COF are 2448 $m^2 g^{-1}$, 1.13 $cm^3 g^{-1}$ and 1381 $m^2 g^{-1}$, 0.59 $cm^3 g^{-1}$, respectively. In contrast, Py-TAPD-COF and Py-Py-COF exhibit a steep uptake in the low-pressure region (P/P_0 < 0.05), revealing their microporous characteristic (Figure 3c and 3d). The PSD analysis

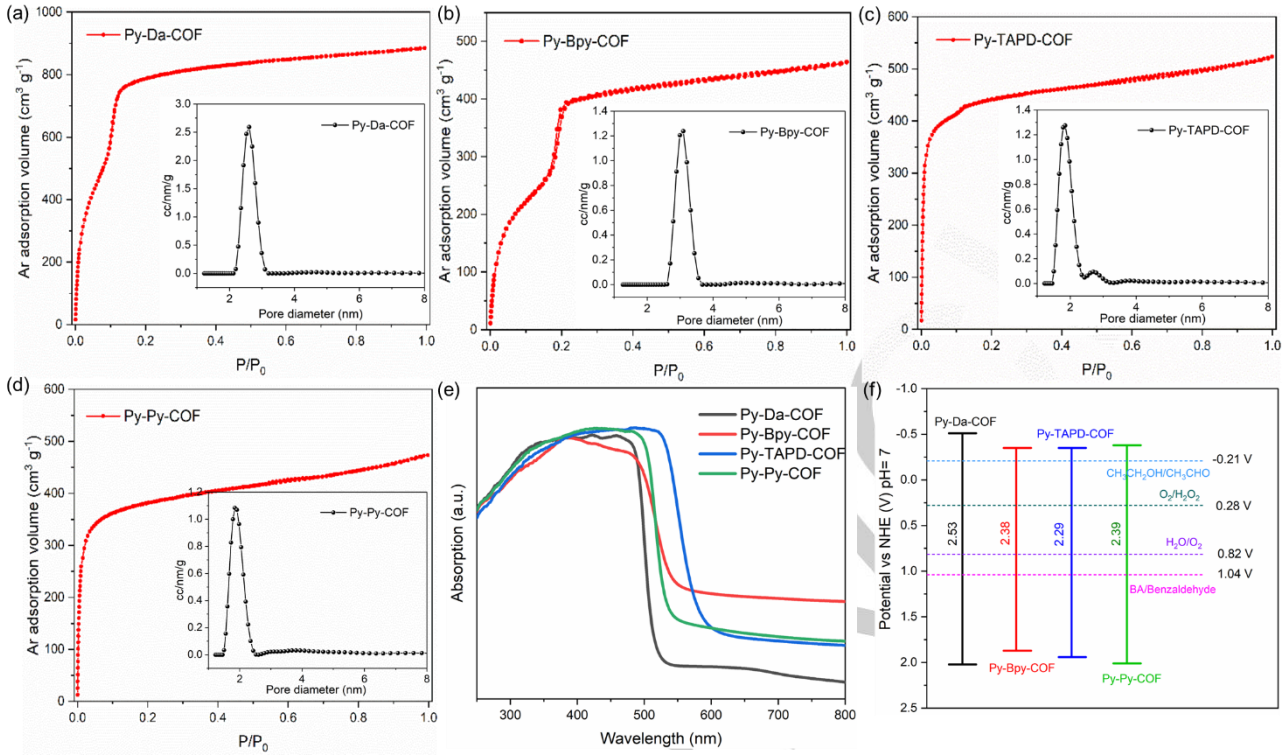

Figure 3. Ar sorption isotherms and pore size distributions (inset) of (a) Py-Da-COF, (b) Py-Bpy-COF, (c) Py-TAPD-COF, and (d) Py-Py-COF. (e) Solid-state UV-vis spectra and (f) band gaps of the pyrene-based COFs.

shows (large) micropores of 1.8 nm for Py-TAPD-COF and 1.9 nm for Py-Py-COF, which correspond well with the simulated values (1.6 and 1.7 nm). The BET surface area and total pore volume (at P/P_0 = 0.99) of Py-TAPD-COF and Py-Py-COF are 1214 m^2 g^{-1}, 0.66 cm^3 g^{-1} and 1059 m^2 g^{-1}, 0.60 cm^3 g^{-1}, respectively. Overall, the BET surface areas decreased in the order of Py-Da-COF > Py-Bpy-COF > Py-TAPD-COF > Py-Py-COF. The large BET surface areas ensure a high surface availability of the active pyrene sites for ORR and accelerate the mass transfer.[14]

The light-harvesting properties of four COFs were evaluated by means of solid-state UV-vis diffuse reflectance spectroscopy. All four COFs display a strong and broad absorption peak in the visible light region (Figure 3e). Cyclic voltammetry measurements were performed to determine valence band (VB) and conduction band (CB) positions (Figure S9). Py-Da-COF, Py-Bpy-COF, Py-TAPD-COF, and Py-Py-COF exhibit VB and CB at 2.02 V/-0.51 V, 2.03 V/-0.35 V, 1.94 V/-0.35 V, and 2.01 V/-0.38 V vs. NHE, respectively. Accordingly, the band gaps of Py-Da-COF, Py-Bpy-COF, Py-TAPD-COF, and Py-Py-COF were calculated to be 2.53, 2.38, 2.29, and 2.39 eV. As CB positions are more negative than -0.33 V and 0.28 V (vs. NHE at pH=7), they are thermodynamically capable of producing H_2O_2 via a direct or indirect $2e^-$ ORR pathway (Figure 3f). Also, we evaluated the charge transfer resistance by electrochemical impedance spectroscopy (EIS), and the separation efficiency of photogenerated electrons and holes by photocurrent response as well as photoluminescence spectroscopy. The properties of the charge transfer resistance as well as the electron and hole separation efficiency show a similar trend, i.e. Py-TAPD-COF> Py-Py-COF> Py-Da-COF> Py-Bpy-COF (Figure S10-S11).

The photocatalytic performance of the COFs for H_2O_2 generation was evaluated under visible light irradiation (420-700 nm). Initially, the experiments were performed in O_2-saturated water in the absence of any sacrificial agents. As shown in Figure 4a, the Py-Da-COF displays the highest rate (461 µmol g^{-1}) for H_2O_2 generation in one hour. Py-Bpy-COF and Py-TAPD-COF show a reasonable photoactivity of 241 and 142 µmol g^{-1}, respectively whereas only 47 µmol g^{-1} H_2O_2 was detected for Py-Py-COF. The H_2O_2 production increased steadily over 3 hours of irradiation to 868, 480, 361, and 85 µmol g^{-1} for Py-Da-COF, Py-Bpy-COF, Py-TAPD-COF, and Py-Py-COF, respectively. In general, the introduction of an electron donor (hole scavenger) in water could improve the rate of H_2O_2 formation by circumventing the slow rate-limiting water oxidation half-reaction.[4] So, the photocatalytic H_2O_2 production was also tested in the presence of ethanol (water: ethanol = 9:1), a commonly used sacrificial agent for $2e^-$ ORR. As shown in Figure 4b, all the COFs display a higher H_2O_2 production rate in the water-ethanol media compared to the sole water system (Figure 4a vs. 4b). Py-Da-COF and Py-Bpy-COF produce H_2O_2 with a rate of 682 µmol g^{-1} and 452 µmol g^{-1} in one hour. After three hours, the cumulative amount of H_2O_2 is 1238 µmol g^{-1} and 866 µmol g^{-1}, respectively. On the contrary, for Py-TAPD-COF and Py-Py-COF, the H_2O_2 generation rate is not significantly enhanced in the presence of ethanol. Cooper *et al.* examined several TAPD-based COFs for photocatalytic H_2O_2 generation and all these COFs showed a rate below 100 µmol g^{-1} h^{-1}.[2d] When correlating the photocatalytic activity with the characteristic of electron and hole separation, no clear straightforward relationships are found. Similar results were observed by Cooper *et al.* for H_2O_2 production using COFs and conjugated polymers.[2d, 4] But it should be mentioned that the photocatalytic performance of the as-prepared COFs is positively correlated to their BET surface area in both systems (water and water-ethanol). It is well known that materials with higher surface areas manifest a better adsorption of reactants and intermediates,

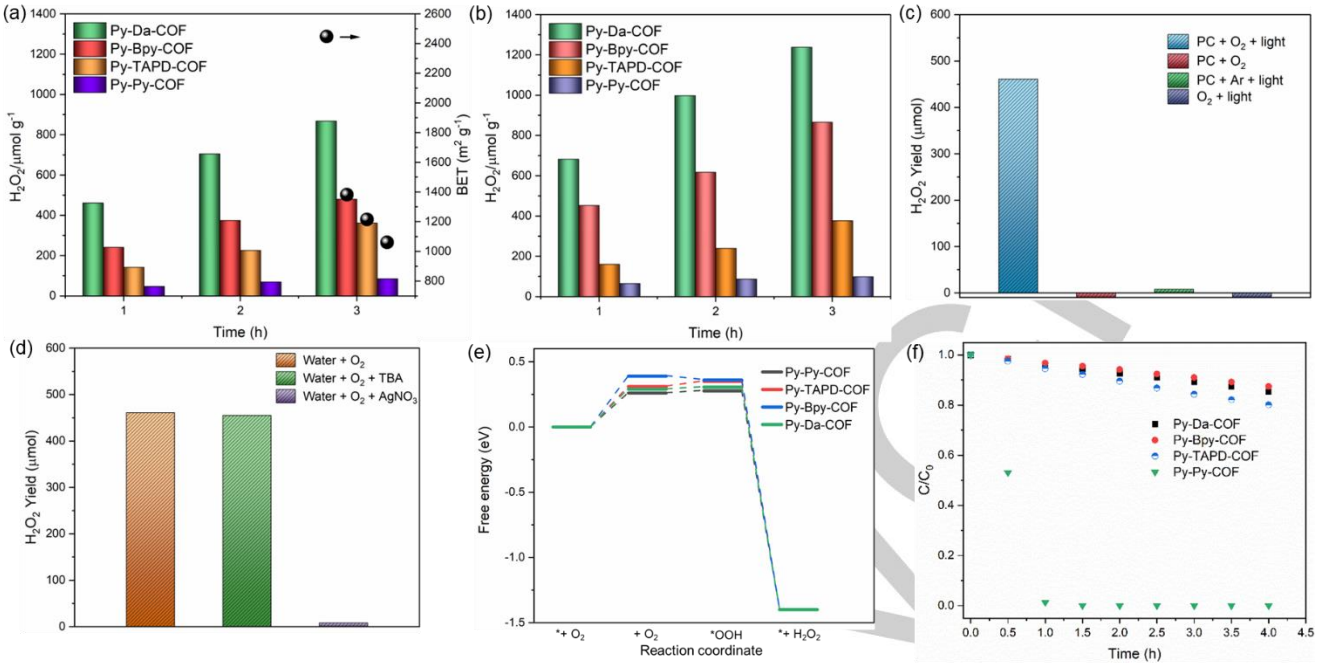

Figure 4. Photoactivity of the COFs for H_2O_2 production in (a) water, (b) water-ethanol (9:1). Photoactivity of Py-Da-COF (c) under different reaction conditions; (d) in the presence of different scavengers (3 mM), one hour irradiation. (e) Calculated reaction free energy for H_2O_2 formation from O_2 at the PBE-D3(BJ) level of theory. (f) Time course of H_2O_2 decomposition (5 mM, initial H_2O_2 concertation) on COFs under light irradiation.

and charge transfer occurs more efficiently.[6b] Furthermore, the high porosity can shorten the diffusion distance of oxygen molecules by allowing them to diffuse directly to the active sites through a cross-plane, thereby enhancing mass transfer.[14a] For example, Shiraishi *et al.* observed that mesoporous g-C_3N_4 (160 m^2 g^{-1}) displayed a much higher H_2O_2 generation activity compared to that of the bulk one (10 m^2 g^{-1}).[15] Similar results were observed by Wu *et al.* for the photocatalytic activity of a CTF,[5a] while in the work of Han *et al.*,[6a] a fluorinated COF exhibited a higher photoactivity for H_2O_2 generation due to its higher surface area. In our case, Py-Da-COF with the highest surface area and the largest total pore volume displays the best photoactivity for H_2O_2 generation. The apparent quantum yield (AQY) was evaluated to be 2.4% (water: ethanol = 9:1) and 4.5% (water: benzyl alcohol = 9:1) at 420 nm for Py-Da-COF, which is a satisfying photoactivity compared to other reported COFs (Table S4). The SCC efficiency in pure water (no sacrificial agents) was calculated to be 0.09% for Py-Da-COF. To further verify the important role of surface areas on photocatalytic performance, Py-TPh-COF which has a similar structure as Py-Da-COF but a lower BET surface area, was synthesized by condensation of Py-CHO with 4,4''-Diamino-p-terphenyl (TPh-NH_2).[16] PXRD, FT-IR, and Ar sorption characterizations were used to confirm that Py-TPh-COF was successfully synthesized (Figure S12-S13). According to the QSDFT analysis, Py-TPh-COF shows mesopores of 3.5 nm. BET surface area and total pore volume at P/P_0 = 0.99 are 649 m^2 g^{-1} and 0.34 cm^3 g^{-1}, which are lower than Py-Da-COF (2448 m^2 g^{-1} and 1.13 cm^3 g^{-1}). Then, the photoactivity of Py-TPh-COF for H_2O_2 generation was evaluated. The Py-TPh-COF produces H_2O_2 with a rate of 167 and 223 μmol g^{-1} h^{-1} in water and water-ethanol systems respectively (Figure S14), which are lower than the rates under the same reaction conditions over Py-Da-COF (461 and 682 μmol g^{-1} h^{-1}). These results jointly endorse our claim that the surface area is an important effect for catalytic activity in our case.

Furthermore, the 2e$^-$ ORR process of the COFs was further confirmed by rotating disk electrode (RED). The average electron transfer numbers of Py-Da-COF, Py-Bpy-COF, Py-TAPD-COF, and Py-Py-COF are 1.72, 1.80, 1.68 and 1.82, respectively (Figure S16). The H_2O_2 production via a 2e$^-$ ORR can occur through two possible pathways: a direct 2e$^-$ (one-step two-electron process) and an indirect 2e$^-$ ORR route (two-step one-electron process via an $\cdot O_2^-$ intermediate).[2c] To investigate the reaction mechanism, a series of control experiments was performed in water. Initially, the importance of light, oxygen, and the need for a photocatalyst (PC, Py-Da-COF in our case) was confirmed. As shown in Figure 4c, no H_2O_2 was detected without light or PC, which means that the H_2O_2 production is a photocatalytic process. When the oxygen was replaced by Ar, only trace amounts of H_2O_2 were produced, meaning the 2e$^-$ ORR is the primary process for H_2O_2 production. Furthermore, the active intermediate was verified by introducing different scavengers, *i.e.*, benzoquinone (BQ, $\cdot O_2^-$ scavenger), $AgNO_3$ (e$^-$ scavenger), and tert-butyl alcohol (TBA, ·OH scavenger) (Figure 4d). $AgNO_3$ strongly suppressed the H_2O_2 production, suggesting that photogenerated electrons are involved in the ORR process. Also, no H_2O_2 was produced in the presence of BQ, which means that $\cdot O_2^-$ participates in the formation of H_2O_2 (see Figure S17, the peroxide levels were evaluated using peroxide test sticks as BQ absorbs light at 409 nm). In contrast, the H_2O_2 production was almost unchanged when TBA was added, meaning that ·OH is not involved in the process of H_2O_2 generation. Based on these control experiments, one can conclude that Py-Da-COF follows the indirect 2e$^-$ ORR mechanism via an $\cdot O_2^-$ intermediate for photocatalytic H_2O_2 generation. Consistent with this mechanism, electron paramagnetic spectroscopy (EPR) experiments show the production of ·OOH adducts upon light irradiation for all COFs (Figure S18). To understand whether the reaction is surface-

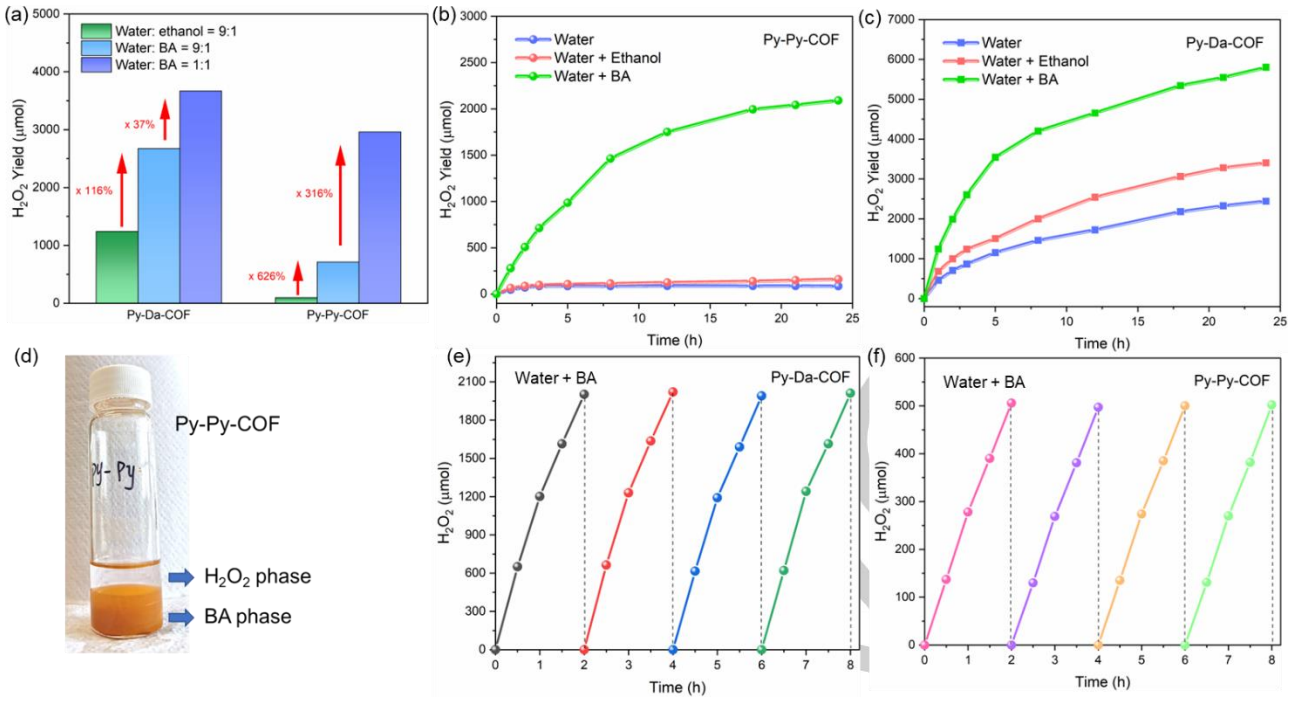

Figure 5. (a) Photoactivity of the COFs for H_2O_2 production after three hours of irradiation in different systems: water: ethanol = 9:1 (5 mL, 5 mg COF; one-phase system); water: BA = 9:1 (5 mL, 5 mg COF; two-phase system); water: BA = 1:1 (10 mL, 5 mg COF; two-phase system); Time course of H_2O_2 accumulation with (b) Py-Py-COF and (c) Py-Da-COF in water, water-ethanol, and water-BA (9:1) systems. (d) Image of Py-Py-COF dispersed in water-BA system (1:1, 10 mL). The recyclability of (e) Py-Da-COF and (f) Py-Py-COF in water-BA (9:1) system.

adsorption-controlled or diffusion-controlled, we performed EIS analyses of all four COFs in water in the presence of O_2. For each COF, we performed EIS measurements at respective CB and at *ca.* CB±0.1V potential to understand the influences of the electron transfer process. The Nyquist and Bode plots obtained from those analyses show interesting insights (Figure S19-S20). It can be noted that the charge transfer resistance (R_{CT}) values of each COF significantly dropped by changing the bias potential from CB+0.1V to CB to CB-0.1V (Table S5). This is a clear indication of the enhanced charge transfer from the material to the medium. More interestingly, significant capacitive behavior can be observed for all four COFs in every bias potential from the Bode plots. This clearly indicates a charged double-layer formation on the catalyst surface endorsing an adsorption behavior, i.e., the reaction is proceeding in an adsorption-controlled manner. This further justifies the coherence of the computed adsorption trend and the experimental catalytic activity of the COFs. As the ORR is happening at the CB, we argue that water is being oxidized at the VB to O_2 (i.e., oxygen evolution reaction or OER) as a counter-reaction to complete the redox process. As an experimental corroboration of this claim, we performed an electrochemical analysis of Py-Da-COF in aqueous and non-aqueous (acetonitrile) media. The polarization curve (Figure S21) in acetonitrile medium provides the electrochemical oxidative potential of the material itself, whereas it in water shows its water oxidation performance. It can be seen that Py-Da-COF manifests impressive OER performance in its VB window (highlighted in green). The onset potential for water oxidation is *ca.* 1.75 V (*vs* NHE), suggesting that the reaction is indeed the $4e^-$ OER, as opposed to the $2e^-$ water oxidation to H_2O_2 which starts at a much higher potential (onset 1.76 V in theory, often >2.0 V in practice with state-of-the-art materials). This was further visually endorsed by the appearance of O_2 bubbles on the electrode surface. As an auxiliary proof, we carried out a set of controlled photoreactions under N_2 atmosphere using $AgNO_3$ as an electron scavenger in deaerating water to push water oxidation at the VB of the COFs. Gas chromatography (GC) analysis (Figure S22) validates the presence of O_2 in the reaction headspace, indicating the generation of O_2. Similar results were observed for the other three COFs. These experiments jointly endorse our claim that the COFs catalyze $2e^-$ ORR at the CB and $4e^-$ OER at the VB in pure water. Based on these results, a plausible reaction mechanism is proposed in Figure S23. Moreover, the binding strength of *OOH intermediate on the pyrene unit (site 1) was evaluated by DFT calculations (* indicating adsorbed state). The free energy of ($H^+ + e^-$) is considered by employing the computational hydrogen electrode model as proposed by Nørskov *et al*.[17] The calculated energy for *OOH intermediate on site 1 of Py-Da-COF is lower than that of Py-TAPD-COF and Py-Bpy-COF, as shown in Figure 4e, indicating Py-Da-COF is more active for H_2O_2 generation, which is consistent with the experimental results. The Py-Da-COF with a higher surface area and a higher amount of pyrene unit (1.31 mmol pyrene g^{-1}_{COF}) shows a better photoactivity for H_2O_2 generation than Py-Bpy-COF (1.09 mmol pyrene g^{-1}_{COF}) and Py-TAPD-COF (0.98 mmol pyrene g^{-1}_{COF}). Surprisingly, the Py-Py-COF exhibits a significantly lower activity compared to Py-Bpy-COF and Py-TAPD-COF, despite having a similar surface area, more active pyrene units (1.79 mmol pyrene g^{-1}_{COF}), and the strongest binding interaction with *OOH intermediate (Figure 4e). We argue that the formed H_2O_2 decomposes over Py-Py-COF in contrast to its desorption from the catalyst surface and diffusion into water.[2c, 18] For this reason, we measured the H_2O_2 decomposition in the presence of the COFs under light irradiation. Before the test, the reaction system was purged with Ar to exclude H_2O_2 generation via the ORR under light irradiation. As shown in Figure 4f, Py-Da-COF and Py-Bpy-COF show a similar

decomposition rate towards H_2O_2, whereas only trace amounts of H_2O_2 are detected after one hour in the presence of Py-Py-COF. In other words, Py-Py-COF exhibits the highest H_2O_2 decomposition rate. This explains why the lowest yield of H_2O_2 is detected when Py-Py-COF is utilized as a photocatalyst. It indicates that COFs with electron-rich pyrene units are beneficial for the $2e^-$ ORR but a high amount of pyrene units in close proximity induces severe H_2O_2 decomposition. To further validate this, the adsorption energy of H_2O_2 molecule over the four COFs was evaluated by DFT (Table S6 and Figure S24). Including three O_2 adsorption sites (as Figure 1), the imine group was also considered for the adsorption of H_2O_2. Our results reveal that the adsorption of H_2O_2 molecule is more favorable at the imine group compared to the other three sites for all the COFs. In comparison at the imine group, Py-Py-COF shows the largest H_2O_2 adsorption energy, meaning the strongest interaction with H_2O_2 molecules, and thus poor desorption. Moreover, electrochemical analysis of the COFs in 5 mM aqueous H_2O_2 solution also confirmed that Py-Py-COF shows significant H_2O_2 reduction within its CB window compared to the other three materials (Figure S25). These experimental findings and the theoretical calculations collectively endorse our aforementioned hypothesis.

To overcome this issue, a two-phase reaction system composed of water and benzyl alcohol (BA) was employed and BA simultaneously acts as a hole scavenger. The COFs are hydrophobic materials that spontaneously disperse in the BA phase while the formed H_2O_2 is present in the water phase. An experiment was performed in a two-phase system with a 9:1 ratio of water and BA, which is the same ratio as for the water-ethanol system. For comparison, Py-Py-COF and Py-Da-COF were evaluated in the water-BA system. As shown in Figure 5a, the cumulative amount of H_2O_2 after three hours of irradiation over Py-Py-COF in the water-BA system (712 µmol g^{-1}) increased by a factor of 6 compared to that in the water-ethanol system (98 µmol g^{-1}), whereas only a 2-fold increment over Py-Da-COF under the same reaction conditions was observed. To verify that the phase separation effect of BA is more prominent than its effect as a hole scavenger agent, we have performed a control experiment in an acetonitrile-BA medium (single phase) where BA only acts as a hole scavenger (Figure S26). The Py-Py-COF produces 186 µmol g^{-1} of H_2O_2 after three hours irradiation, which is lower than that in a water-BA medium (712 µmol g^{-1}) under the same reaction conditions. The result confirms the significant effect of the two-phase reaction system. To obtain a better dispersion of Py-Py-COF in the BA phase, the ratio of water and BA was decreased from 9:1 to 1:1. Compared to the water-BA system with a 9:1 ratio, Py-Py-COF has a 316% rate increase (from 712 to 2961 µmol g^{-1}) in a 1:1 ratio of water and BA system which is 8.5 times greater than that of Py-Da-COF (37%, from 2673 to 3670 µmol g^{-1}). The results suggest that in the two-phase system, the H_2O_2 decomposition is strongly suppressed because the active sites of COFs remain in the BA phase whereas the formed H_2O_2 quickly diffuses into the water. This allows for an increase in the concentration of H_2O_2 in the water phase.

The long-term photostability of materials was evaluated and a continuous 24-hour experiment was performed in the three systems using Py-Da-COF and Py-Py-COF. As shown in Figure 5b and 5c, both COFs exhibit the highest H_2O_2 production activities in the two-phase system. The photocatalytic activity of Py-Py-COF in the two-phase system improved significantly compared to that of Py-Da-COF, which is consistent with the aforementioned results. Moreover, it is seen that the accumulation of H_2O_2 is still increasing gradually over continuous 24 hours of irradiation, meaning that COFs are still capable to produce H_2O_2 after continuous 24-hour irradiation, although the rate slows down as a function of time. However, we performed recycling experiments with the same catalysts and fresh substrates. Upon recycling up to four runs, the initial rates of formation of H_2O_2 are very similar in each run (Figure 5e, 5f, and S27-S28), suggesting the good stability and recyclability of the photocatalysts. To confirm the structure integrity of the spent COFs, PXRD and FTIR measurements were performed. No obvious changes are observed in the PXRD and FTIR patterns of the spent catalysts (Figure S29-S34) compared to those of the fresh materials, which means their structures are retained well after a long-time run or four successive runs.

Conclusion

In summary, we performed a systematic study on the pyrene-based COFs for the efficient production of H_2O_2. Our results confirmed that pyrene units are the most active reduction centers over the other sites. Besides, the well-distribution of active centers over a large surface area plays an important role in enhancing the photocatalytic performance. The reported findings highlight that the presence of pyrene active sites in very close proximity leads to unwanted H_2O_2 decomposition. Accordingly, we employed a biphasic system (benzyl alcohol and water) in which the COF disperses in the benzyl alcohol and the produced H_2O_2 quickly diffuses into the water layer, inhibiting H_2O_2 decomposition. A H_2O_2 production rate of 1242 µmol g^{-1} h^{-1} was achieved and the catalyst is stable and durable. We believe that careful structural design combined with appropriate reaction conditions are promising avenues to achieve highly efficient systems for photocatalysis.

Acknowledgements

J.M.S. acknowledges the financial support from Ghent University (BOF CSC preference program 01SC0619). J.M.S. and H.C. acknowledge the financial support of the China Scholarship Council (CSC, 201906060159). S.A. acknowledges the financial support from Ghent University (01D04318). The authors acknowledge the financial support from the FWO (I002418N) and Ghent University through a Concerted Research Action (GOA010-17). The computational resources (Stevin Supercomputer Infrastructure) and services used in this work were provided by the VSC (Flemish Supercomputer Center), funded by Ghent University, FWO and the Flemish Government – department EWI.

Keywords: Covalent organic frameworks, Pyrene, Photocatalysis, Oxygen reduction, Hydrogen peroxide generation

[1] L. X. Wang, J. J. Zhang, Y. Zhang, H. G. Yu, Y. H. Qu, J. G. Yu, *Small* **2022**, *18,* 2104561-2104582.

[2] a) M. Melchionna, P. Fornasiero, M. Prato, *Adv. Mater.* **2019**, *31,* 1802920-1802924; b) R. Ciriminna, L. Albanese, F. Meneguzzo, M. Pagliaro, *ChemSusChem* **2016**, *9*, 3374-3381; c) X. K. Zeng, Y. Liu, X. Y. Hu, X. W. Zhang, *Green Chemistry* **2021**, *23*, 1466-1494. d) W. Zhao, P. Yan, B. Li,

M. Bahri, L. Liu, X. Zhou, R. Clowes, N. D. Browning, Y. Wu, J. W. Ward, A. I. Cooper, *J. Am. Chem. Soc.* **2022**, *22*, 9902-9909.

[3] Y. Y. Sun, L. Han, P. Strasser, *Chem. Soc. Rev.* **2020**, *49*, 6605-6631.

[4] L. J. Liu, M. Y. Gao, H. F. Yang, X. Y. Wang, X. B. Li, A. I. Cooper, *J. Am. Chem. Soc.* **2021**, *143*, 19287-19293.

[5] a) L. Chen, L. Wang, Y. Y. Wan, Y. Zhang, Z. M. Qi, X. J. Wu, H. X. Xu, *Adv. Mater.* **2020**, *32,* 1904433-1904442; b) X. H. Yu, B. Viengkeo, Q. He, X. Zhao, Q. L. Huang, P. P. Li, W. Huang, Y. G. Li, *Adv. Sustain. Syst.* **2021**, *5,* 2100184-2100190.

[6] a) H. Z. Wang, C. Yang, F. S. Chen, G. F. Zheng, Q. Han, *Angew. Chem. Int. Edit.* **2022**, *61,* e202202328; b) L. J. Li, L. P. Xu, Z. F. Hu, J. C. Yu, *Adv. Funct. Mater.* **2021**, *31,* 2106120-2106128; c) M. P. Kou, Y. Y. Wang, Y. X. Xu, L. Q. Ye, Y. P. Huang, B. H. Jia, H. Li, J. Q. Ren, Y. Deng, J. H. Chen, Y. Zhou, K. Lei, L. Wang, W. Liu, H. W. Huang, T. Y. Ma, *Angew. Chem. Int. Edit.* **2022**, *61,* e202200413; d) C. Krishnaraj, H. S. Jena, L. Bourda, A. Laemont, P. Pachfule, J. Roeser, C. V. Chandran, S. Borgmans, S. M. J. Rogge, K. Leus, C. V. Stevens, J. A. Martens, V. Van Speybroeck, E. Breynaert, A. Thomas, P. Van der Voort, *J. Am. Chem. Soc.* **2020**, *142*, 20107-20116.

[7] H. Wang, H. Wang, Z. W. Wang, L. Tang, G. M. Zeng, P. Xu, M. Chen, T. Xiong, C. Y. Zhou, X. Y. Li, D. N. Huang, Y. Zhu, Z. X. Wang, J. W. Tang, *Chem. Soc. Rev.* **2020**, *49*, 4135-4165.

[8] L. Zhai, Z. Xie, C.-X. Cui, X. Yang, Q. Xu, X. Ke, M. Liu, L.-B. Qu, X. Chen, L. Mi, *Chem. Mater.* **2022**, *49*, 5232-5240.

[9] a) F. P. Kinik, A. Ortega-Guerrero, D. Ongari, C. P. Ireland, B. Smit, *Chem. Soc. Rev.* **2021**, *50*, 3143-3177; b) J. X. Jiang, A. Trewin, D. J. Adams, A. I. Cooper, *Chemical Science* **2011**, *2*, 1777-1781; c) G. Cheng, T. Hasell, A. Trewin, D. J. Adams, A. I. Cooper, *Angew. Chem. Int. Edit.* **2012**, *51*, 12727-12731.

[10] X. Y. Yan, D. H. Li, L. X. Zhang, X. J. Long, D. J. Yang, *Appl. Catal. B-Environ.* **2022**, *304,* 120908-120916.

[11] a) S. Wang, Q. Sun, W. Chen, Y. Q. Tang, B. Aguila, Y. X. Pan, A. M. Zheng, Z. Y. Yang, L. Wojtas, S. Q. Ma, F. S. Xiao, *Matter* **2020**, *2*, 416-427; b) L. Stegbauer, S. Zech, G. Savasci, T. Banerjee, F. Podjaski, K. Schwinghammer, C. Ochsenfeld, B. V. Lotsch, *Adv. Energy Mater.* **2018**, *8,* 1703278-1703285; c) G. J. Xiao, W. Q. Li, T. Chen, W. B. Hu, H. Yang, Y. A. Liu, K. Wen, *Eur. J. of Org. Chem.* **2021**, *2021*, 3986-3991.

[12] a) L. Ascherl, E. W. Evans, M. Hennemann, D. Di Nuzzo, A. G. Hufnagel, M. Beetz, R. H. Friend, T. Clark, T. Bein, F. Auras, *Nat. commun.* **2018**, *9,* 3802-3807; b) A. F. M. EL-Mahdy, M. G. Mohamed, T. H. Mansoure, H. H. Yu, T. Chen, S. W. Kuo, *Chem. Commun.* **2019**, *55*, 14890-14893; c) Z. Lu, H. J. Yang, X. L. Fu, Y. L. Zhao, L. Q. Xiao, Z. F. Zhang, L. X. Hou, *Macromol. Rapid Comm.* **2021**, *42*, 2100384-2100391; d) E. Q. Jin, K. Y. Geng, K. H. Lee, W. M. Jiang, J. Li, Q. H. Jiang, S. Irle, D. L. Jiang, *Angew. Chem. Int. Edit.* **2020**, *59*, 12162-12169.

[13] X. Y. Wang, L. J. Chen, S. Y. Chong, M. A. Little, Y. Z. Wu, W. H. Zhu, R. Clowes, Y. Yan, M. A. Zwijnenburg, R. S. Sprick, A. I. Cooper, *Nat. Chem.* **2018**, *10*, 1180-1189.

[14] a) H. Wang, X. Liu, P. Niu, S. L. Wang, J. Shi, L. Li, *Matter* **2020**, *2*, 1377-1413; b) D. H. Yang, Y. Tao, X. S. Ding, B. H. Han, *Chem. Soc. Rev.* **2022**, *51*, 761-791.

[15] Y. Shiraishi, Y. Kofuji, H. Sakamoto, S. Tanaka, S. Ichikawa, T. Hirai, *ACS Catal.* **2015**, *5*, 3058-3066.

[16] T. A. Wang, I. F. Azhar, Y. T. Yang, Y. Lu, Y. Y. Tian, N. Gao, F. C. Cui, L. Yang, X. F. Jing, G. S. Zhu, *Nano. Res.* **2022**, *15*, 4569-4574.

[17] J. K. Norskov, J. Rossmeisl, A. Logadottir, L. Lindqvist, J. R. Kitchin, T. Bligaard, H. Jonsson, *J. Phys. Chem. B* **2004**, *108*, 17886-17892.

[18] J. H. Lee, H. Cho, S. O. Park, J. M. Hwang, Y. Hong, P. Sharma, W. C. Jeon, Y. Cho, C. Yang, S. K. Kwak, H. R. Moon, J. W. Jang, *Appl. Catal. B-Environ.* **2021**, *284,* 119690-119700.

Table of Contents

Four highly porous pyrene-based covalent organic frameworks (COFs) were prepared for photocatalytic H_2O_2 generation. The reported findings highlight that the presence of pyrene active sites in very close proximity leads to unwanted H_2O_2 decomposition. Accordingly, a biphasic system (benzyl alcohol and water) was employed to inhibit H_2O_2 decomposition.